The 7th International Supercritical CO_2 Power Cycles Symposium
Feb. 21 – 24, 2022, San Antonio, Texas
Paper #173

Identifying Cost-Effective Steels for Direct-Fired sCO_2 Power Cycles

Richard P. Oleksak*
Contracting Research Scientist
National Energy Technology Laboratory
Albany, OR USA
*Richard.Oleksak@netl.doe.gov

Joseph H. Tylczak
Research Metallurgist (Retired)
National Energy Technology Laboratory
Albany, OR USA
thermocouple@hotmail.com

Casey S. Carney
Contracting Research Scientist
National Energy Technology Laboratory
Albany, OR USA
Casey.Carney@netl.doe.gov

Reyixiati Repukaiti
Graduate Researcher
National Energy Technology Laboratory
Albany, OR USA
Reyixiati.Repukaiti@netl.doe.gov

Ömer N. Doğan
Materials Research Engineer
National Energy Technology Laboratory
Albany, OR USA
Omer.Dogan@netl.doe.gov

Richard Oleksak is a Contracting Research Scientist working with the Structural Materials Team in the Research & Innovation Center at NETL. He received his Ph.D. from Oregon State University in Chemical Engineering in 2015. His research focuses on materials issues for current and future clean energy technologies.

Casey Carney is a Contracting Research Scientist working with the Structural Materials Team in the Research & Innovation Center at NETL. He received his Ph.D. from the University of Colorado Boulder in Chemical Engineering in 2005. His work includes high temperature corrosion issues with advanced fossil fueled power systems.

Joseph Tylczak is a Research Metallurgist Engineer in the Structural Materials Team in the Research & Innovation Center at NETL. He received his degree in Physical Metallurgy from Washington State University in 1979. His work includes high temperature corrosion issues with advanced fossil fueled power systems and ambient temperature corrosion of gas transmission pipelines. Joseph retired in February 2021.

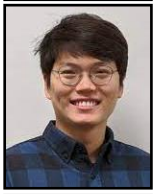

Reyixiati Repukaiti is an Oakridge Institute for Science and Education (ORISE) Graduate Scholar working with the Structural Materials Team in the Research & Innovation Center at NETL. He received his Ph.D. from Oregon State University in Materials Science & Engineering in 2021. His research focuses on understanding corrosion behavior of alloys in advanced energy systems.

Ömer Doğan is a Materials Research Engineer in the Structural Materials Team in the Research & Innovation Center at NETL. He received his Ph.D. from Case Western Reserve University in Materials Science & Engineering in 1990. Current research focuses on the evaluation and development of heat, corrosion, and wear resistant materials for applications in harsh environments.

ABSTRACT

Environmental compatibility remains a primary concern for materials selection in supercritical CO_2 (sCO_2) power cycles. This is especially true for direct-fired cycles operated by the oxy-combustion of fossil fuels, where other components of the working fluid such as H_2O, O_2, along with impurities such as SO_2, increase corrosion concerns. Little is known about the chemical compatibility of candidate structural alloys in these impure CO_2-rich environments. As a result, relatively expensive austenitic stainless steels (e.g., 300 series steels such as 316) are currently being employed in these systems to ensure sufficient environmental resistance, even for relatively low temperatures (<450 °C). Identification of less expensive steels that can be used at these low-to-intermediate temperatures may offer considerable cost savings. In this work, we investigated the compatibility of a variety of steels, including cost-effective (low Ni) 400 series steels, in both the CO_2-rich gas/supercritical phase, as well as the carbonic acid-saturated aqueous phase, expected in direct-fired sCO_2 cycles. Multiple steels are shown to be compatible and therefore should be considered as promising candidate materials for construction of direct-fired sCO_2 power systems.

INTRODUCTION

When surveying possible steel construction materials for supercritical CO_2 (sCO_2) power cycles, the first requirement is that the steel possesses acceptable mechanical properties, such as creep strength, at the temperatures and pressures of interest. A second but equally important requirement is that the steel is compatible with the corrosive CO_2-rich environments found in the temperature regimes of the cycle where the steel would be used. In general, steels become more expensive as the mechanical and corrosion performance improves. Hence, informed materials selection involves a trade-off of performance and cost, where the goal is to determine the least expensive steel which will exhibit acceptable performance over the lifetime of the component. This optimization is especially important for heat exchangers, which may represent up to 90% of the materials cost of an sCO_2 power cycle [1]. Ni-based superalloys will likely be used at temperatures above approximately 650 °C due to their very high creep strength. Below 650 °C, different grades of steels may be employed because they are substantially less expensive than Ni-based alloys. As a result, many research groups over the last decade have investigated the behavior of candidate steels in both pure (indirect cycle) [2-14] and impure (direct cycle) [15-18] CO_2 environments. The vast majority of these studies have focused on temperatures near the maximum use temperature of the steels, approximately 550-650 °C. Alternatively, very little work has focused on compatibility at lower temperatures [19-21]. Because of the limited compatibility data of steels at these lower temperatures, some current sCO_2 demonstration plants have employed relatively expensive 18Cr-10Ni stainless steels such as 316 down to the lowest temperatures of the plant to ensure adequate environmental resistance. An improved understanding of steel compatibility at these low to intermediate temperatures (≈50-450 °C) is needed to enable informed selection of cost-effective materials to reduce the cost of building future power plants. This paper describes ongoing efforts at the National Energy Technology Laboratory to achieve this goal, with an emphasis on the environments expected in direct-fired (impure) sCO_2 cycles.

EXPERIMENTAL

The compositions of the steels used in this study are shown in Table 1. Rectangular samples were machined from the steel plates. The samples used for 450 °C (gaseous) and 550 °C (supercritical) exposures were 19 mm × (8-13 mm) × (0.9-2.9 mm) and were surface finished through 600 grit SiC paper (CAMI designation). The samples used for the 50 °C (aqueous) exposures were 30 mm × 20 mm × 2 mm and were surface finished through 1200 grit SiC paper (CAMI designation). Two or three replicate samples were used in all exposure tests and the reported error represents one standard deviation. The samples were dimensioned, ultrasonically cleaned in acetone and/or alcohol, and weighed prior to (and after) exposure using a semi-micro analytical balance with 0.01 mg precision.

Table 2 summarizes the different exposure environments used in this study and the intended purpose of the exposure, i.e., the component being simulated. The experimental details for the 450 °C atmospheric pressure (tube furnace) exposures are available in the references noted in Table 2. In short, the tube furnace exposure environments consisted of high purity (99.999%) CO_2 (henceforth "aCO_2"), CO_2 containing 4% H_2O and 1% O_2 (henceforth "DF4"), and CO_2 containing 4% H_2O, 1% O_2, and 0.1% SO_2 (henceforth "DF4S").

The 550 °C supercritical exposure (henceforth "sDF4") was performed in a vertical autoclave constructed of alloy 230 (Marks Brothers) heated with three zone temperature control (Thermcraft). Pressurized high purity (99.999%) CO_2 and reverse osmosis deionized H_2O flows

were provided with liquid pumps (Supercritical Fluid Technologies models SFT-10 and Series II, respectively). A blend of 20% O_2/Ar was injected into the pressurized flow with a pneumatic booster pump (Haskel AG-75). Samples were suspended vertically in the autoclave and purged ten times using Ar with 0.7 MPa to 0.2 MPa cycles. The autoclave was heated at 200 °C/h to 450 °C, then at 100 °C/h to 550 °C. Upon reaching temperature, liquid CO_2 was injected at a rate of 6 mL/min until a pressure of 20.0 MPa was reached. Once the system reached pressure, the CO_2 flow was reduced to 2 mL/min and the water and O_2/Ar flows were started to achieve a fluid composition (mol%) equivalent to the DF4 tube furnace exposure described above, i.e., 95% CO_2, 4% H_2O, and 1% O_2. At this flow rate the autoclave volume was replenished approximately every 50-60 min. Oxygen concentration was monitored downstream (ambient pressure), with an inline O_2 analyzer (MTI Corporation EQ-W1000-LD). Samples were exposed in 500 h increments; at the conclusion of each increment the system was de-pressurized and furnace cooled overnight before removing the samples for weighing, then reloading the samples for continued exposure by repeating the above procedure.

The aqueous exposures were done by emerging samples in 750 mL of solution in a 1100 mL static autoclave. Samples were tightly fitted on a polytetrafluoroethylene (PTFE) rod with spaces between samples to prevent galvanic corrosion. The solution consisted of aerated deionized water without or with 0.5 mM H_2SO_4. After loading the samples, the autoclave was heated and pressurized to 50 °C and 8 MPa simultaneously using 99% CO_2 and 1% O_2, then held at these conditions for 96 hours. The exposures without and with H_2SO_4 addition are henceforth referred to as carbonic acid and carbonic/sulfuric acid exposures, respectively. Sampling small volumes of solution throughout the exposures indicated a pH of approximately 4.3 and 3.3 for the carbonic acid and carbonic/sulfuric acid exposures, respectively. Because minimal corrosion product formed on the sample surfaces after the experiments, the weight change (i.e., exposed sample mass minus initial sample mass) was assumed to represent metal loss during the exposure and was used to calculate the corrosion rates reported in this paper.

After the exposures, select samples were cross-sectioned and polished to a 1 µm diamond finish then analyzed using an FEI Inspect F Scanning Electron Microscope (SEM) at an accelerating voltage of 5-20 kV. All SEM images were collected in backscattered electron (BSE) mode.

RESULTS AND DISCUSSION

Figure 1 shows the mass change of several different steels after 2500 h exposure to three different CO_2-rich environments at 450 °C and atmospheric pressure (0.1 MPa). A temperature of 450 °C was chosen because it represents the approximate maximum use temperature of the 400-series steels (409, 410, 416, 420, 430) included in this study. The steels are listed in Fig. 1 in order of increasing Cr content (see Table 1). Figure 1a shows results in high purity CO_2. The purpose of this exposure was to establish a baseline to understand the effects of impurities and higher pressures expected in a real direct-fired sCO_2 system, as described further below. A clear transition is seen in Fig. 1a where all steels with Cr content up to and including 10.5 wt% (SAVE12) showed high mass gains, whereas all steels with Cr greater than or equal to 11.5 wt% (409) showed much lower mass gains. The origin of this mass gain behavior is illustrated by cross-sectional SEM images of four of the steels (Grade 91, 410, 430, 347H) in Fig. 2. The left column in Fig. 2 shows the steels exposed to high purity CO_2. Figure 2a indicates that Grade 91 (and other steels with <11.5 wt% Cr) formed an Fe-rich oxide scale. Fe-oxides grow at a fast rate [22], which resulted in a relatively thick (≈25 µm) scale for Grade 91 after 2500 h. Alternatively, Fig. 2d, 2g, and 2j indicate that 410, 430, and 347H (and all

other steels with ≥11.5 wt% Cr) contained enough Cr to form a Cr-rich oxide scale in high purity CO_2. The growth rate of Cr-rich oxides is much slower than Fe-oxides [22], resulting in a much thinner scale for these steels. The insets in Fig. 2 show the Cr-rich oxide scales at higher magnification, indicating they were approximately 0.25 µm thick for the steels that formed them in high purity CO_2, approximately two orders of magnitude thinner compared to the Fe-rich oxide scale formed on Grade 91. While the precise oxidation rates that will be acceptable for a steel will depend on the component geometry and required lifetime, a possible scenario is that Fe-rich oxide growth will be unacceptable, while Cr-rich oxide growth represents acceptable "protective" behavior. In addition to faster scale growth rates, Fe-rich oxides also allow significant carbon uptake by the steel from the CO_2-rich environment [23, 24], which can embrittle the steel and reduce its creep strength [25-27], whereas Cr-rich oxides significantly limit the amount of carbon uptake by the steel [28]. Hence, identifying the critical level of Cr required for the steel to form a Cr-rich oxide is seen to be an important metric for material selection from an environmental compatibility perspective.

Figure 1b and 1c show the mass change of the same steels at the same temperature (450 °C), pressure (0.1 MPa), and time (2500 h) but in the presence of the impurities expected in a direct-fired sCO_2 power cycle [6]. Specifically, the CO_2-rich environment containing 4% H_2O and 1% O_2 ("DF4") is intended to simulate the composition expected by the combustion of (sulfur-free) natural gas. Meanwhile, the environment containing the same water and oxygen content with an additional 0.1% SO_2 ("DF4S") is intended to simulate the composition expected by the combustion of coal syngas in the absence of a sulfur removal process. Figure 1b shows that the level of Cr required to form a Cr-rich oxide is increased in the presence of 4% H_2O and 1% O_2 in the gas. That is, 409, 410, 420, 416, and L80 all showed higher mass gains compared to tests in pure CO_2, whereas only steels with greater than or equal to 16.3 wt% Cr (i.e., 430 and higher Cr steels) showed low mass gains. The SEM images in Fig. 2b, 2h, and 2k confirm that the steels with low mass gains (430 and 347H) formed a thin Cr-rich oxide scale, whereas the steel with high mass gain (Grade 91) formed a thick Fe-rich oxide scale. Meanwhile, Fig. 2e indicates that 410, which showed an intermediate mass gain, existed intermediate these two regimes, where most of the surface was covered by Fe-rich oxide while a small portion of the surface developed a thin Cr-rich oxide.

Interestingly, the situation was slightly improved by the addition of 0.1% SO_2. Figure 1c shows that L80 (13.1 wt% Cr) experienced the very low mass gains characteristic of fully protective behavior, while several additional steels containing slightly lower levels of Cr (409, 410, 420, 416) also showed lower mass gains compared to the SO_2-free condition. The corresponding SEM images (Fig. 2c, 2f, 2i, 2l) largely confirm the reaction products expected from the mass gains, where Grade 91 formed exclusively thick Fe-rich oxide, 430 and 347H formed exclusively thin Cr-rich oxide, and 410 formed some amount of Fe-rich oxide (to an extent that was lower compared to the SO_2-free condition). The positive effect of SO_2 impurities at 450 °C is contrary to results of the same exposure environments at 550 °C, where the presence of SO_2 increased the mass gains of high-Cr steels (such as 347H) compared to the SO_2-free condition [29]. This highlights that the effect of SO_2 on the oxidation behavior of the steels can be highly dependent on the exposure temperature [15]. Prior work studying oxyfuel combustion environments has likewise highlighted the complex effect of SO_2 impurities on the oxidation behavior of steels in high-temperature CO_2-rich gases [30-35].

To explore the combined effects of impurities and high pressure, several of the same (plus additional) steels are being exposed to the SO_2-free condition at 20 MPa ("sDF4") in a flowing autoclave. These exposures are being done at 550 °C and so are not directly comparable to the 450 °C tests described above, however they are comparable to prior tests of several of the

same steels exposed to the DF4 gas at 550 °C and 0.1 MPa [29]. Figure 3 shows the mass changes of the steels after 2000 h, including a comparison for the six steels (Grade 22, Grade 91, 347H, 304H, 310S, E-Brite) that were previously tested at 0.1 MPa [29]. The mass change results for the 20 MPa exposure indicate a relatively strong effect of pressure, where both 347H (which showed artificially low mass gain due to scale spallation) and 304H did not show the same protective behavior at 20 MPa that they showed at 0.1 MPa. Interestingly, the (ferritic) steel with the highest Cr level of 26.5 wt% (E-Brite) also showed a relatively high mass gain of 0.3 mg/cm^2, whereas the three austenitic steels with Cr between 19.9 and 25.0 wt% (800, 309H, 310S) showed the lowest mass gains (<0.1 mg/cm^2). These results indicate that pressure can have a strong effect on the oxidation behavior of the steels and that higher Cr levels may be required for protective behavior in real direct-fired sCO_2 systems compared to results of laboratory studies at atmospheric pressure. This is in moderate agreement with limited additional studies in high pressure (supercritical) CO_2 containing lower levels of oxygen and water impurities, where pressure did show a negative effect for some steels [17]. Characterization of samples exposed at 20 MPa is planned upon completion of the exposure to better understand this relatively strong effect of pressure.

The above results provide useful information on the compatibility of different types of steels in the intermediate temperature (450-550 °C) portions of a direct-fired sCO_2 power cycle where steel degradation occurs essentially by a gas phase oxidation process. It is important to recognize that if a steel that is deemed compatible at these intermediate temperatures is employed for the remaining lower temperature portions of the cycle, it will encounter an environment where the mechanism of degradation changes significantly. Specifically, at temperatures below ≈100 °C (depending on the pressure and fluid composition [36]) liquid water will precipitate from the supercritical phase. This aqueous phase, which is in contact with the high-pressure CO_2-rich supercritical phase, will be saturated with CO_2, producing a carbonic acid (H_2CO_3) environment. The aqueous phase will also contain dissolved oxygen due to the presence of O_2 in the supercritical phase. Finally, if sulfur is present, it will likewise partition to the aqueous phase and produce sulfuric acid (H_2SO_4). In fact, the sulfuric acid dew point (≈100-250 °C depending on pressure and composition) is higher than that of water, which raises the possibility of concentrated sulfuric acid within a narrow temperature range of the cycle, before liquid water precipitates and dilutes the acid. This poses a unique acid dew point corrosion concern that must be addressed if sulfur is present [37]. This environment was not simulated in the present study. Instead, the environments produced after the precipitation of water, both for the condition with and without sulfur, were simulated herein using static autoclaves.

Figure 4 shows the corrosion rates (from the measured mass losses) of four of the steels after exposure to the oxygenated carbonic acid and carbonic/sulfuric acid mixtures expected in the low temperature portions of a direct-fired sCO_2 power cycle without and with sulfur impurities, respectively. As with the oxidation experiments, the aqueous corrosion behavior of the steels shows a clear dependence on Cr content. This effect is well known and reflects the increased ability of the steel to form a passive oxide/hydroxide film when the Cr content is increased [38]. For example, 347H forms a Cr-rich oxyhydroxide film with a thickness of less than 5 nm in oxygenated carbonic acid solution at 50 °C after 500 h [39]. The corrosion rates were not strongly affected by the presence of dilute H_2SO_4, suggesting sulfur does not exacerbate corrosion concerns in the low temperature aqueous phase. Again, the precise corrosion rate that will be acceptable is dependent on the component geometry and required lifetime, however rates above 0.01 mm/year may be unacceptable, particularly for thin sectioned components. By this metric, both 430 and 347H exhibit acceptably low corrosion rates whereas lower Cr steels are more susceptible to degradation in this aqueous phase.

SUMMARY AND CONCLUSIONS

Several commercially available steels were exposed to environments simulating the operating conditions of the intermediate and low temperature portions of a direct-fired sCO_2 power cycle. As expected, the Cr content of the steel was a primary factor which determined compatibility both in the intermediate temperature (450-550 °C) oxidizing environments and low temperature (50 °C) aqueous corrosion environments. Compared to pure CO_2, additions of water and oxygen increased the Cr content that was required for protective behavior at 450 °C. Nevertheless, multiple steels were still found to be compatible, including 430 and 347H. Flowing autoclave tests containing water and oxygen at 550 °C suggested that pressure does play a role, where higher Cr contents were required for protective behavior compared to previously reported atmospheric pressure tests. Additional experiments are needed to determine if this trend holds true at 450 °C. Low temperature corrosion tests indicated that 430 and 347H were likewise compatible in the oxygenated acidic aqueous phases expected at the lowest temperatures of the cycle, whereas lower Cr steels may exhibit unacceptably high corrosion rates at these conditions.

A primary incentive of this work was to identify cost-effective steels for direct-fired sCO_2 power cycles. An important conclusion is that 400-series steels, especially those with relatively high Cr content such as 430, may be acceptable materials up to their maximum use temperatures of ≈450 °C, which could represent a significant reduction in material cost. At temperatures of 550 °C, our study shows that even 18Cr-10Ni steels (such as 347) may not contain sufficient Cr for impure CO_2 environments at high (realistic) system pressures. Meanwhile, some steels with both high Cr content and strength (such as 310 and 800) are relatively expensive due to large quantities of Ni (19 and 31 wt%, respectively). At these temperatures 309, which has relatively high Cr (22 wt%), similar strength compared to 310, and relatively little Ni (12 wt%), may represent a desirable trade-off of performance and cost.

REFERENCES

[1] D. Fleming, J. Pasch, T. Conboy, M. Carlson, Testing platform and commercialization plan for heat exchanging systems for sCO_2 power cycles, in: ASME Turbo Expo 2013: Turbine Technical Conference and Exposition, American Society of Mechanical Engineers Digital Collection, San Antonio, TX, USA, 2013.

[2] R.P. Oleksak, F. Rouillard, Materials performance in CO_2 and supercritical CO_2, in: R.J.M. Konings, R.E. Stoller (Eds.) Comprehensive Nuclear Materials 2nd Edition, Oxford: Elsevier, 2020, pp. 422-451.

[3] V. Firouzdor, K. Sridharan, G. Cao, M. Anderson, T.R. Allen, Corrosion of a stainless steel and nickel-based alloys in high temperature supercritical carbon dioxide environment, Corrosion Science, 69 (2013) 281-291.

[4] H.J. Lee, H. Kim, S.H. Kim, C. Jang, Corrosion and carburization behavior of chromia-forming heat resistant alloys in a high-temperature supercritical-carbon dioxide environment, Corrosion Science, 99 (2015) 227-239.

[5] F. Rouillard, T. Furukawa, Corrosion of 9-12Cr ferritic–martensitic steels in high-temperature CO_2, Corrosion Science, 105 (2016) 120-132.

[6] J.P. Shingledecker, S.C. Kung, I.G. Wright, Predicting the Oxidation/Corrosion Performance of Structural Alloys in Supercritical CO_2, Electric Power Research Institute, 2017, pp. 1-206.

[7] R.P. Oleksak, J.H. Tylczak, C.S. Carney, G.R. Holcomb, Ö.N. Doğan, High-Temperature Oxidation of Commercial Alloys in Supercritical CO_2 and Related Power Cycle Environments, JOM, 70 (2018) 1527–1534.

[8] R.I. Olivares, D.J. Young, T.D. Nguyen, P. Marvig, Resistance of High-Nickel, Heat-Resisting Alloys to Air and to Supercritical CO_2 at High Temperatures, Oxidation of Metals, 90 (2018) 1-25.

[9] B. Adam, L. Teeter, J. Mahaffey, M. Anderson, L. Árnadóttir, J.D. Tucker, Effects of Corrosion in Supercritical CO_2 on the Microstructural Evolution in 800H Alloy, Oxidation of Metals, 90 (2018) 453–468.

[10] B.A. Pint, R. Pillai, M.J. Lance, J.R. Keiser, Effect of Pressure and Thermal Cycling on Long-Term Oxidation in CO_2 and Supercritical CO_2, Oxidation of Metals, 94 (2020) 505–526.

[11] Y. Gui, Z. Liang, H. Shao, Q. Zhao, Corrosion behavior and lifetime prediction of VM12, Sanicro 25 and Inconel 617 in supercritical carbon dioxide at 600 °C, Corrosion Science, 175 (2020) 108870.

[12] M.H.S. Bidabadi, S. Chandra-ambhorn, A. Rehman, Y. Zheng, C. Zhang, H. Chen, Z.-G. Yang, Carbon Depositions within the Oxide Scale and its Effect on the Oxidation Behavior of Low Alloy Steel in Low (0.1 MPa), Sub-(5 MPa) and Supercritical (10 MPa) CO_2 at 550 °C, Corrosion Science, 177 (2020) 108950.

[13] R.P. Oleksak, C.S. Carney, L. Teeter, Ö.N. Doğan, Oxidation Behavior of Welded Fe-Based and Ni-Based Alloys in Supercritical CO_2, Oxidation of Metals, (2021) 1-17.

[14] X. Guo, Z. Liu, L. Li, J. Cheng, H. Su, L. Zhang, Revealing the long-term oxidation and carburization mechanism of 310S SS and Alloy 800H exposed to supercritical carbon dioxide, Materials Characterization, 183 (2022) 111603.

[15] R.P. Oleksak, J.H. Tylczak, Ö.N. Doğan, High-Temperature Oxidation of Steels in Direct-Fired CO_2 Power Cycle Environments, JOM, 73 (2021) 3965–3973.

[16] S. Kung, J. Shingledecker, I. Wright, T. Lolla, A. Sabau, Corrosion of Heat Exchanger Alloys in Open-Fired sCO_2 Power Cycles, in: Proceedings of 6th International Supercritical CO_2 Power Cycles Symposium, Pittsburgh, Pennsylvania, 2018.

[17] B.A. Pint, J. Lehmusto, M.J. Lance, J.R. Keiser, Effect of pressure and impurities on oxidation in supercritical CO_2, Materials and Corrosion, 70 (2019) 1400-1409.

[18] K. Li, Y. Zeng, J.-L. Luo, Corrosion of SS310 and Alloy 740 in high temperature supercritical CO_2 with impurities H_2O and O_2, Corrosion Science, 184 (2021) 109350.

[19] A. Brittan, J. Mahaffey, M. Anderson, Corrosion and Mechanical Performance of Grade 92 Ferritic-Martensitic Steel After Exposure to Supercritical Carbon Dioxide, Metallurgical and Materials Transactions A, 51 (2020) 2564–2572.
[20] B.A. Pint, R. Pillai, J.R. Keiser, Compatibility of Steels in Supercritical CO_2 at 450°-550°C, in: 2020 NACE CORROSION Conference, NACE International, Virtual, 2020.
[21] B.A. Pint, R. Pillai, J.R. Keiser, Effect of Supercritical CO_2 on Steel Ductility at 450°-650°C, in: ASME Turbo Expo 2021, ASME, Virtual, 2021.
[22] D.J. Young, High Temperature Oxidation and Corrosion of Metals, 2nd ed., Elsevier, 2016.
[23] T. Gheno, D. Monceau, J. Zhang, D.J. Young, Carburisation of ferritic Fe–Cr alloys by low carbon activity gases, Corrosion Science, 53 (2011) 2767-2777.
[24] F. Rouillard, G. Moine, M. Tabarant, J.C. Ruiz, Corrosion of 9Cr Steel in CO_2 at Intermediate Temperature II: Mechanism of Carburization, Oxidation of Metals, 77 (2012) 57-70.
[25] S.R. Akanda, R.P. Oleksak, R. Repukaiti, K.A. Rozman, Ö.N. Doğan, Effect of Specimen Thickness on the Degradation of Mechanical Properties of Ferritic-Martensitic P91 Steel by Direct-fired Supercritical CO_2 Power Cycle Environment, Metallurgical and Materials Transactions A, 52 (2021) 82-93.
[26] S.R. Akanda, R.P. Oleksak, R. Repukaiti, K.A. Rozman, Ö.N. Doğan, Effect of Thickness on Degradation of Austenitic 347H Steel by Direct-fired Supercritical CO_2 Power Cycle Environment Corrosion Science, 192 (2021) 109795.
[27] K.A. Rozman, R.P. Oleksak, Ö.N. Doğan, M. Detrois, P.D. Jablonski, J.A. Hawk, Creep of MARBN-type 9Cr martensitic steel in gaseous CO_2 environment, Materials Science and Engineering: A, 826 (2021) 141996.
[28] R.P. Oleksak, G.R. Holcomb, C.S. Carney, L. Teeter, Ö.N. Doğan, Effect of Surface Finish on High Temperature Oxidation of Steels in CO_2, Supercritical CO_2 and Air, Oxidation of Metals, 92 (2019) 525–540.
[29] R.P. Oleksak, J.H. Tylczak, G.R. Holcomb, Ö.N. Doğan, High temperature oxidation of steels in CO_2 containing impurities, Corrosion Science, 164 (2020) 108316.
[30] P. Huczkowski, T. Olszewski, M. Schiek, B. Lutz, G.R. Holcomb, V. Shemet, W. Nowak, G. Meier, L. Singheiser, W.J. Quadakkers, Effect of SO_2 on oxidation of metallic materials in CO_2/H_2O-rich gases relevant to oxyfuel environments, Materials and Corrosion, 65 (2014) 121-131.
[31] C. Yu, T.D. Nguyen, J. Zhang, D.J. Young, Corrosion of Fe–9Cr–(Mn, Si) alloys in CO_2–H_2O–SO_2 gases, Corrosion Science, 98 (2015) 516-529.
[32] C. Yu, T.D. Nguyen, J. Zhang, D.J. Young, Sulfur effect on corrosion behavior of Fe-20Cr-(Mn, Si) and Fe-20Ni-20Cr-(Mn, Si) in CO_2-H_2O at 650 °C, Journal of The Electrochemical Society, 163 (2016) C106-C115.
[33] C. Yu, J. Zhang, D.J. Young, High temperature corrosion of Fe-Cr-(Mn/Si) alloys in CO_2-H_2O-SO_2 gases, Corrosion Science, 112 (2016) 214-225.
[34] C. Yu, J. Zhang, D.J. Young, Corrosion Behaviour of Fe–Cr–(Mn, Si) Ferritic Alloys in Wet and Dry CO_2–SO_2 Atmospheres at 650 °C, Oxidation of Metals, 90 (2018) 97-118.
[35] P. Huczkowski, D.J. Young, T. Olszewski, A. Chyrkin, W.J. Quadakkers, Effect of Sulphur on the Oxidation Behaviour of Possible Construction Materials for Heat Exchangers in Oxyfuel Plants in the Temperature Range 550-700 °C, Oxidation of Metals, 89 (2018) 651-681.
[36] L. Teeter, R. Repukaiti, N. Huerta, R.P. Oleksak, R.B. Thomas, Ö.N. Doğan, M. Ziomek-Moroz, J.D. Tucker, Effect of O_2 on the long-term operation and corrosion of steel X65 in CO_2-H_2O environments for direct supercritical CO_2 power cycle applications, The Journal of Supercritical Fluids, 152 (2019) 104520.
[37] X. Lu, M. McGroddy, B. Forrest, D. Freed, J. Kay, J. Laumb, J. Stanislowski, J. Hurley, Dynamic corrosion tests in a CO_2-rich environment, in: Proceedings of the Materials Science & Technology Conference, Columbus, OH, 2018.
[38] P. Marcus, Corrosion mechanisms in theory and practice, CRC press, 2011.

[39] R.P. Oleksak, J.P. Baltrus, L. Teeter, M. Ziomek-Moroz, Ö.N. Doğan, Characterization of corrosion films formed on austenitic stainless steel in supercritical CO_2 containing H_2O and O_2, Corrosion, 74 (2018) 1047-1053.

ACKNOWLEDGEMENTS

This work was performed in support of the U.S. Department of Energy's Fossil Energy Crosscutting Technology Research Program. We thank Jeffrey Hawk (NETL), Paul Jablonski (NETL), and Martin Detrois (NETL) for providing the NETL developed steels (JMP3, JMP4). We further thank Christopher McKaig (NETL) and Matthew Fortner (NETL) for preparing the sample cross-sections.

DISCLAIMER

Table 1. Compositions of tested alloys (wt%) measured by wavelength dispersive X-ray fluorescence (C contents are nominal values). The steels are listed in order of Cr content. Only Fe and Cr content are listed for JMP3 and JMP4 steels, which are currently under development at NETL. *Composition provided by the manufacturer.

	Alloy	Fe	Ni	Cr	Co	Mo	W	Al	Si	Ti	Mn	Nb	C
Ferritic/Martensitic Steels	**Grade 22***	95.5	0.2	2.3	-	0.9	-	0.03	0.2	-	0.5	-	0.1
	Grade 91*	89.3	0.09	8.4	-	0.9	-	0.01	0.3	-	0.5	0.07	0.09
	JMP3	83.2	-	9.6	-	-	-	-	-	-	-	-	-
	JMP4	82.7	-	10.1	-	-	-	-	-	-	-	-	-
	SAVE 12	82.8	-	10.5	2.9	-	2.9	-	0.2	-	0.5	0.07	0.1
	409	86.8	0.3	11.5	0.03	0.02	-	0.1	0.4	0.2	0.4	0.01	0.08
	410*	86.9	0.4	11.8	-	0.04	-	0.01	0.4	-	0.4	-	0.1
	420	86.0	0.4	12.4	0.02	0.09	0.02	0.05	0.3	0.01	0.5	0.01	0.2
	416	85.5	0.3	12.5	0.02	0.2	0.01	0.01	0.2	0.01	1.1	0.01	0.1
	L80	85.7	0.3	13.1	0.02	-	0.02	0.01	0.2	0.01	0.4	0.01	0.2
	430*	82.5	0.3	16.3	-	0.05	-	-	0.4	-	0.4	-	0.04
	E-Brite	71.6	0.2	26.5	0.02	1.0	-	0.1	0.3	-	0.04	0.1	0.01
Austenitic Steels	**347H***	70.1	9.0	17.3	0.1	0.4	-	-	0.3	-	1.9	0.5	0.05
	304H	70.6	8.3	18.7	0.2	0.1	0.01	0.01	0.4	-	1.1	0.01	0.07
	800	44.2	32.7	19.9	0.07	0.2	-	0.4	0.5	0.5	0.9	0.05	0.1
	309H*	62.9	12.2	22.3	0.2	0.4	-	0.01	0.3	0.01	1.6	-	0.06
	310S*	53.5	19.1	25.0	0.2	0.09	-	0.02	0.4	-	1.4	0.01	0.04

Table 2. Details of the exposure conditions used in this study and their intended purpose (i.e., component being simulated). HX = Heat Exchanger

Test Name	T (°C)	P (MPa)	Composition	Phase	Component Being Simulated	Experimental Details
aCO_2	450	0.1	99.999% CO_2	Gas	Intermediate Temperature HX of Indirect Cycle	Ref [28]
DF4	450	0.1	95%CO_2, 4%H_2O, 1%O_2	Gas	Intermediate Temperature HX of Natural Gas-Fired Direct Cycle	Ref [15]
DF4S	450	0.1	95%CO_2, 4%H_2O, 1%O_2, 0.1%SO_2	Gas	Intermediate Temperature HX of Coal Syngas-Fired Direct Cycle	Ref [15]
sDF4	550	20	95%CO_2, 4%H_2O, 1%O_2	Supercritical Fluid	Intermediate Temperature HX of Natural Gas-Fired Direct Cycle	Experimental Section
Carbonic Acid	50	8	H_2O containing 0.05 mM H_2CO_3 and 1 mM O_2	Aqueous	Low Temperature HX and Water Separator of Natural Gas-Fired Direct Cycle	Experimental Section
Carbonic/ Sulfuric Acid	50	8	H_2O containing 0.05 mM H_2CO_3, 0.5 mM H_2SO_4, 1 mM O_2	Aqueous	Low Temperature HX and Water Separator of Coal Syngas-Fired Direct Cycle	Experimental Section

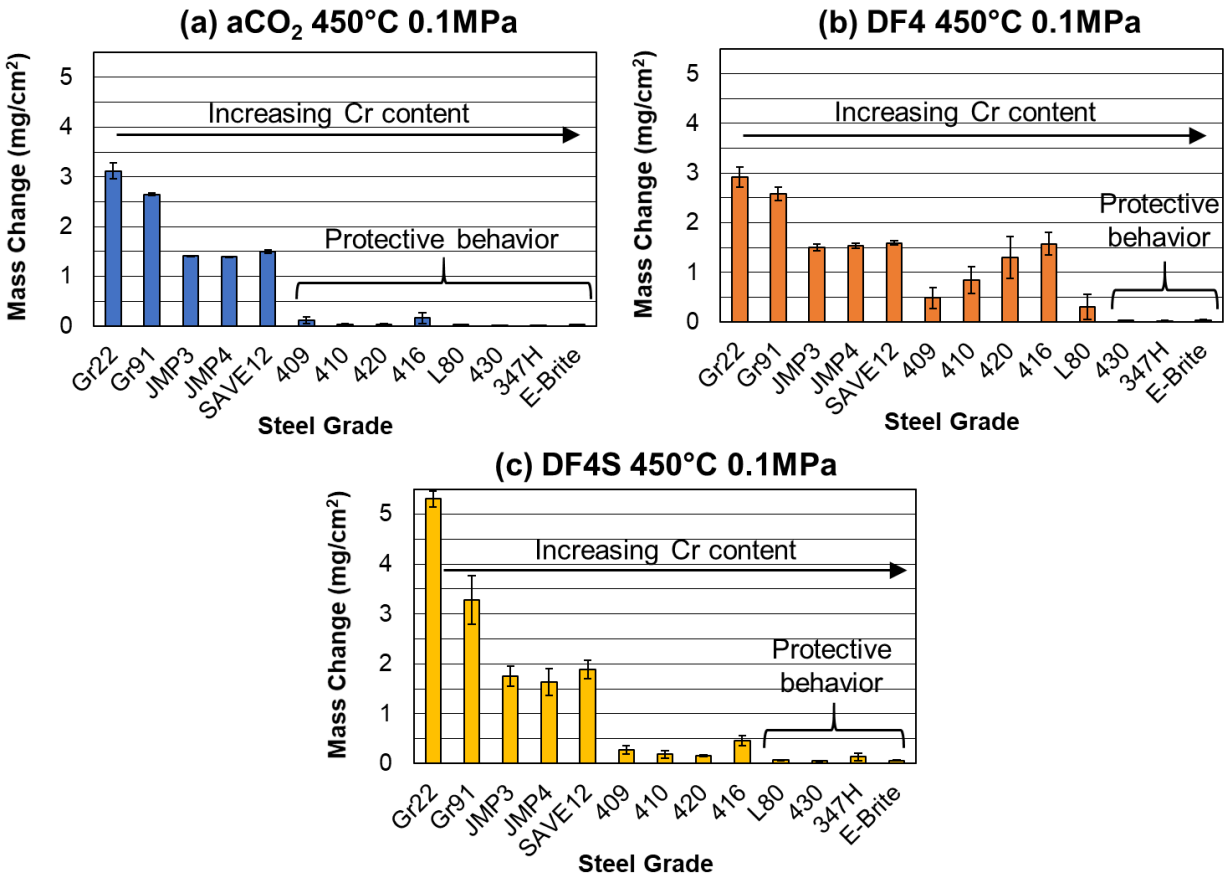

Figure 1. Mass change of several steels after exposure to different CO_2-rich environments at 450 °C and 0.1 MPa for 2500 h (a) "aCO_2" = 99.999% CO_2 (b) "DF4" = 95% CO_2 + 4% H_2O + 1% O_2 (c) "DF4S" = 95% CO_2 + 4% H_2O + 1% O_2 + 0.1% SO_2.

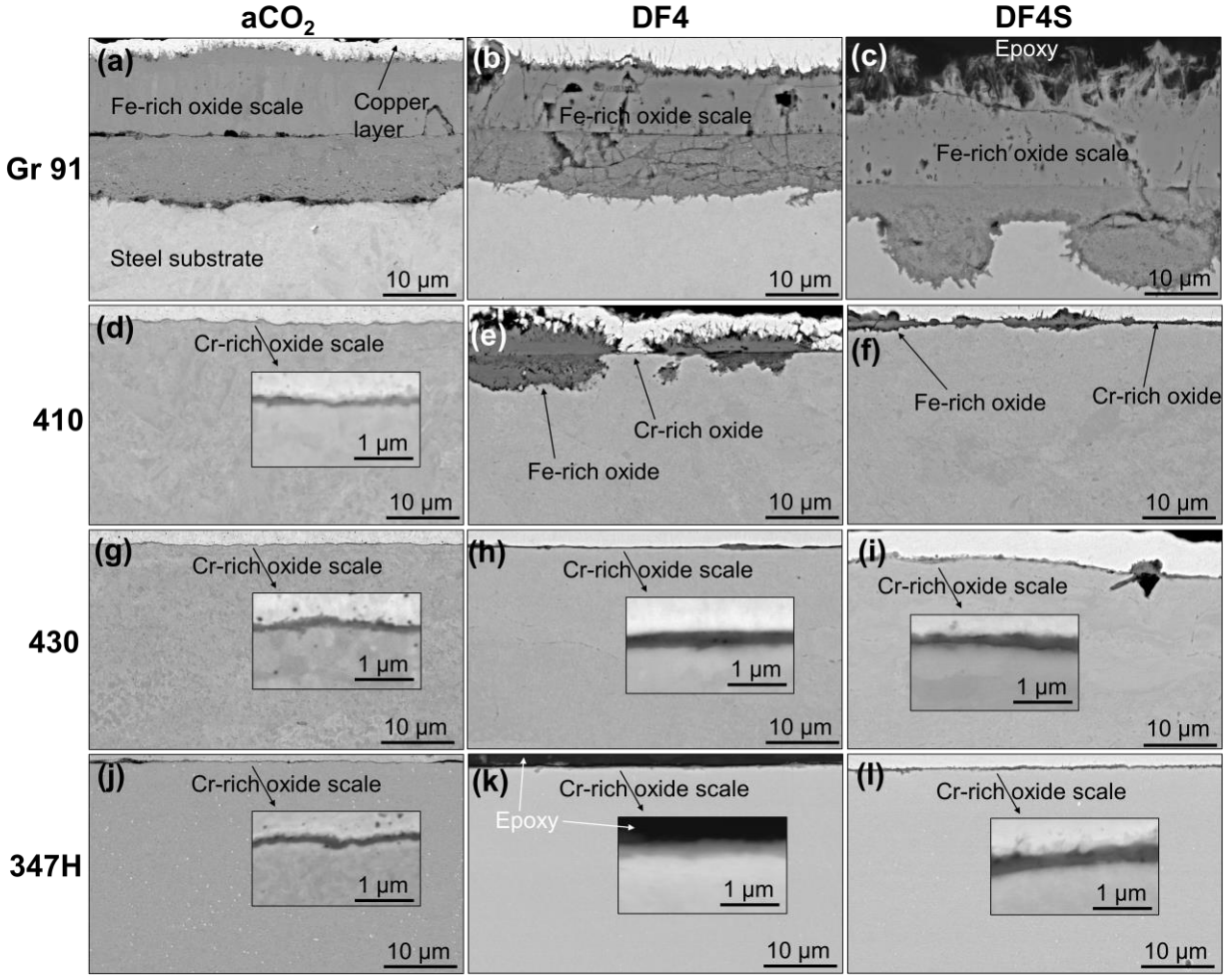

Figure 2. Cross-sectional SEM images showing oxide scales formed on (a-c) Grade 91 steel (d-f) 410 steel (g-i) 430 steel (j-l) 347H steel after exposure to different CO_2-rich environments at 450 °C and 0.1 MPa for 2500 h. "aCO_2" = 99.999% CO_2, "DF4" = 95% CO_2 + 4% H_2O + 1% O_2, "DF4S" = 95% CO_2 + 4% H_2O + 1% O_2 + 0.1% SO_2.

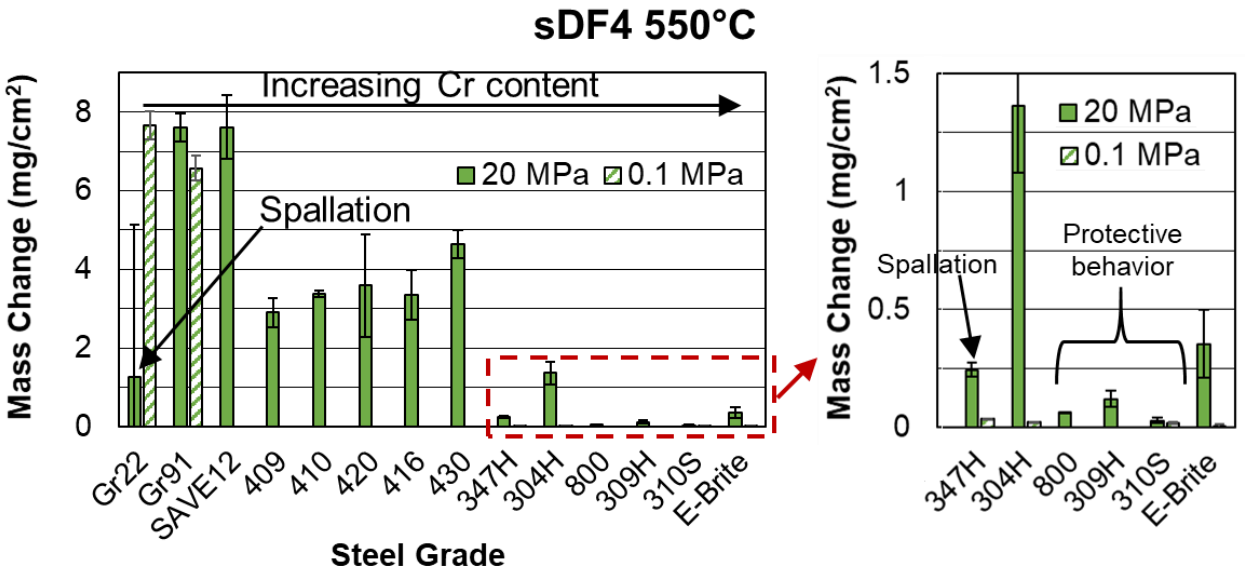

Figure 3. Mass change of several steels after exposure to supercritical environment "sDF4" = 95% CO_2 + 4% H_2O + 1% O_2 at 550 °C and 20 MPa for 2000 h. Six steels (Gr22, Gr91, 347H, 304H, 310S, E-Brite) previously exposed to the same environment at 0.1 MPa are included for comparison [29].

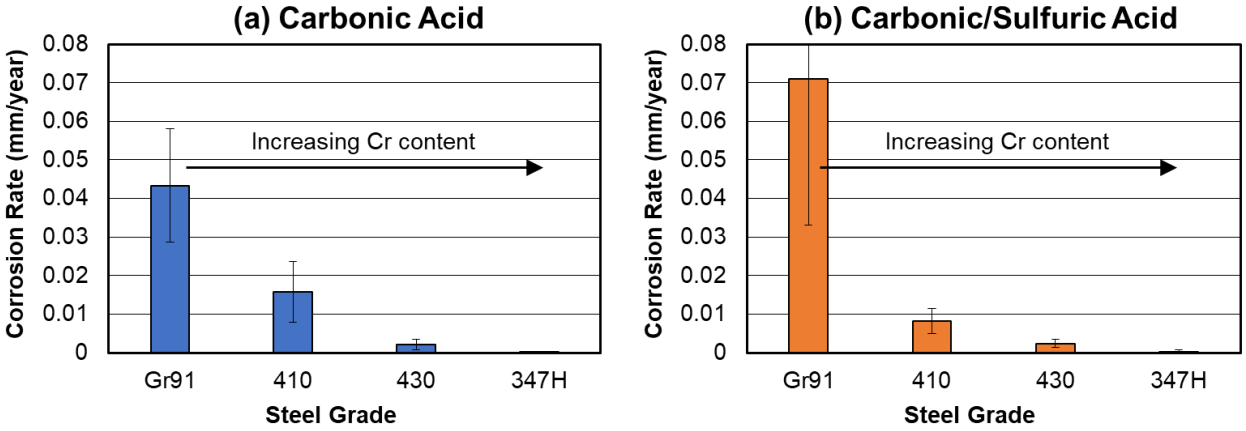

Figure 4. Corrosion rates of different steels determined from 96 h exposures in aqueous solutions of oxygenated carbonic acid and carbonic/sulfuric acid mixture at 50 °C and 8 MPa.